Open access • Journal Article • DOI:10.1016/J.APCATB.2015.10.006

Effect of NaBH4 on properties of nanoscale zero-valent iron and its catalytic activity for reduction of p-nitrophenol — Source link

Sungjun Bae, Suji Gim, Hyungjun Kim, Khalil Hanna

Institutions: École Normale Supérieure, KAIST

Published on: 01 Mar 2016 - Applied Catalysis B-environmental (Elsevier)

Effect of NaBH4 on properties of nanoscale zero-valent iron and its catalytic activity for reduction of p-nitrophenol

Sungjun Bae, Suji Gim, Hyungjun Kim, Khalil Hanna

Effect of $NaBH_4$ on properties of nanoscale zero-valent iron and its catalytic activity for reduction of *p*-nitrophenol

Sungjun Bae,[a] Suji Gim,[b] Hyungjun Kim,[b] and Khalil Hanna[a,*]

[a]École Nationale Supérieure de Chimie de Rennes, UMR CNRS 6226, 11 Allée de Beaulieu, 35708 Rennes Cedex 7, France

[b]Graduate School of Energy, Environment, Water, and Sustainability (EEWS), Korea Advanced Institute of Science and Technology, 291 Daehak-ro, Yuseong-Gu, Daejeon 305-701, Republic of Korea

*Corresponding author: Tel.: +33 2 23 23 80 27; fax: +33 2 23 23 81 20.

E-mail address: khalil.hanna@ensc-rennes.fr (K. Hanna)

Graphical abstract

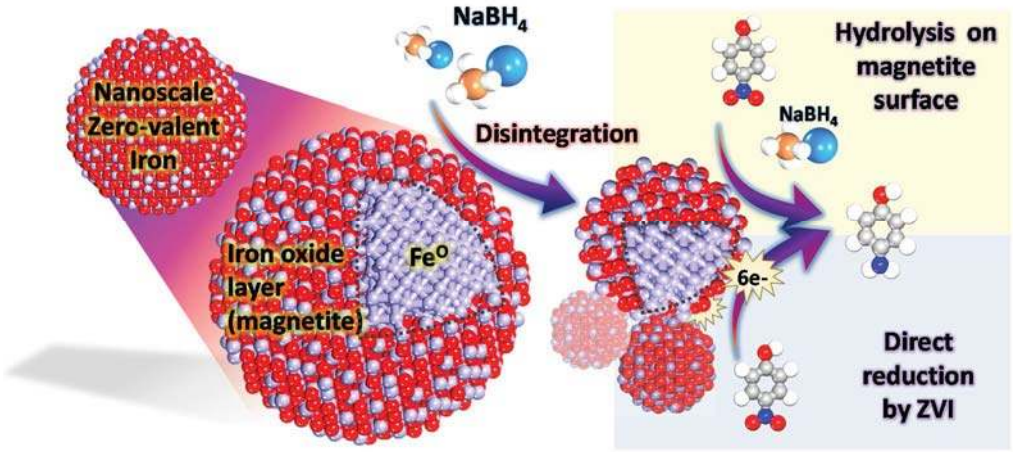

Highlights

- $NaBH_4$ disintegrated NZVI to much smaller sized NZVI.
- NZVI/$NaBH_4$ system showed a remarkable catalytic reduction of p-NP.
- A complete reduction of p-NP was observed during four recycling tests.
- $NaBH_4$ can prevent the oxidation of NZVI during the catalytic reduction process.
- DFT showed magnetite on NZVI also played an important role for p-NP reduction.

Abstract

The reduction of p-Nitrophenol (p-NP) to p-Aminophenol (p-AP) by nanoscale zero-valent iron (NZVI)/ $NaBH_4$ system in an oxygen environment was studied by means of liquid chromatography, spectroscopy (vibration and X-ray photoelectron), solid analyses (transmission electron microscopy and X-ray diffraction) and density functional theory (DFT) calculations. Addition of $NaBH_4$ into NZVI suspension showed the disintegration of NZVI(60-100 nm), resulting in the formation of much smaller particles (15-40 nm) due to the chemical

etching of outermost surfaces (i.e., magnetite). Interestingly, complete reduction of p-NP and high conversion efficiency of p-AP (> 98%) were observed in NZVI/$NaBH_4$ system even after four recycling which is quite comparable with widely used noble metallic catalysts. Surface analysis confirmed that $NaBH_4$ can prevent the oxidation of NZVI surface, leading to the continuous reduction of p-NP in oxygen environments. Experimental results and DFT calculations suggested that not only the formation of smaller NZVI but also thermodynamic preferences for reduction of p-NP on outermost surfaces of NZVI (i.e. magnetite) may significantly affect the reduction process of p-NP in NZVI/$NaBH_4$ system. These novel findings can promote the development of new NZVI technologies which can be used for wastewater reductive treatment in oxygen environments.

Keywords

Nanoscale zero-valent iron; $NaBH_4$; p-Nitrophenol; oxygen environment; density functional theory

1. Introduction

p-Nitropheonol (p-NP) contamination of surface and groundwater has gradually increased due to the excessive consumption of dyes, pesticides, and pharmaceuticals from industrial and agricultural activities [1]. Because it has been considered as one of the toxic organic pollutants responsible for eye and skin irritation and methemoglobinemia potentially causing cyanosis, confusion, and unconsciousness [1,2], United States Environmental Protection Agency set a guideline restricting the contaminant level of p-NP to below 10 ng/L in natural water [3]. There

is therefore an extensive effort to effectively treat the wastewater contaminated by p-NP. Among many treatment technologies, catalytic reduction of p-NP to *p*-Aminophenol (p-AP) in the presence of sodium borohydride ($NaBH_4$) has been intensively investigated [4-11]. This catalytic reaction has become one of the most widely used model reactions due to the easy measurement of both p-NP and p-AP by UV-vis spectroscopy and the complete conversion without production of by-products [12]. Furthermore, the conversion of p-NP to p-AP has great commercial relevance because p-AP is an important intermediate for the manufacture of analgesic/antipyretic drugs, paracetamol, acetanilide, and aniline [13,14].

Since Pradhan et al. have reported the catalytic reduction of p-NP by Ag nanoparticle [15], various noble metallic nanoparticles (i.e., Au, Pt, and Ag) were produced by chemical and biological synthesis [4,5]. These noble metals were usually immobilized on other supports (i.e., carbon materials, polymers, and metal oxides) [5-10] for the effective, stable, and recyclable catalysis for p-NP reduction. However, most noble metals are extremely expensive (despite of its usage in low concentration) and involve potential loss of the noble metals during recycling process. In addition, most synthesis methods of catalysts are usually very complicated, time-consuming, and labored processes. Therefore, it is timely to develop a novel reduction process of p-NP to p-AP, which could be cheap, environmental-friendly, and readily available for all.

Herein, a simple method for conversion of p-NP to p-AP by using NZVI and $NaBH_4$ was developed. In the past two decades, NZVI has attracted a great attention as a promising reactant for reductive removal of various environmental contaminants in agricultural and industrial wastewaters [16-22]. Although NZVI has shown a remarkable reduction potential in laboratory and field studies, most processes performed in anoxic environments due to the rapid surface oxidation of NZVI to iron oxides by oxygen. Furthermore, passivation of NZVI surface is also generally observed during the reduction of contaminants even in anoxic environments [18,20].

Therefore, the surface passivation is one of the urgent problems to be overcome for wide application of NZVI to other oxygen environments.

In this work, a systematic study was performed to investigate the reduction kinetic of p-NP by NZVI with $NaBH_4$ in oxygen environments and its possibility to be repeatedly used in recycling tests. The impact of $NaBH_4$ on NZVI reactivity was evaluated by using a variety of surface analysis techniques, density functional theory (DFT) calculations, and spectrophotometric and chromatographic measurements. The driving mechanism of $NaBH_4$-enhanced reductive ability of NZVI was discussed. We note that, to the best of our knowledge, this is the first study elucidating the effect of $NaBH_4$ on pure NZVI in oxygen environments for simultaneous contaminant degradation with production of useful organic resource.

2. Experimental and theoretical methods

2.1. Chemicals

All chemicals and solvents used in the experiment were of guaranteed analytical grade.

2.2. Synthesis of NZVI and iron minerals

NZVI was synthesized by reducing $FeCl_3 \cdot 6H_2O$ (0.11 M) with $NaBH_4$ solution (0.9 M) in anaerobic chamber (JACOMEX), modifying our previous method [18]. The precipitates in the suspension were washed three times with deaerated deionized water (DDW), prepared using ultra-pure water (18MΩ·cm) purged with N_2 for 4 h, by centrifuging for 5 min at 4000 rpm. NZVI was dried and stored in the anaerobic chamber. Other iron minerals were synthesized and characterized in the context of previous works (goethite (α-$Fe^{III}OOH$) [23], magnetite ($Fe^{II}{}_1{}^{III}{}_2O_4$) [24] and hematite (α-$Fe^{III}{}_2O_3$) [24]). Maghemite was purchased from Sigma-Aldrich (γ-$Fe^{III}{}_2O_3$).

2.3. Reduction of p-NP

NZVI stock suspension (105 mg/L, 1.95 mM) containing in 100 mM $NaBH_4$ was prepared in anaerobic chamber and taken out from anaerobic chamber for reduction experiment in oxygen environment. For the p-NP reduction, 2.6 mL of $NaBH_4$ (50 mM) was added into a quartz cuvette, then 0.1 mL of NZVI stock was added into the cuvette. The aqueous NZVI suspension was sonicated for 3 sec and 0.3 mL of p-NP (1 mM) was transferred into the cuvette to initiate the reduction of p-NP. Total volume of reaction mixture was 3 mL with initial concentrations of 3.5 mg/L NZVI(0.065 mM) and 0.1 mM p-NP. The change in p-NP concentration was monitored at 400 nm wavelength by UV-vis spectrophotometer (CARY 50 probe, Varian). Control test using NZVI (0.065 mM) without $NaBH_4$ showed no reduction of p-NP in oxygen environment (data not shown). For the recycling test, the used NZVI was magnetically collected at the bottom of the cuvette by removing the aqueous solution. Then, collected NZVI was washed with fresh $NaBH_4$ solution (100 mM) twice by magnetic separation as described above. Finally, 2.7 mL of $NaBH_4$ (50 mM) and 0.3 mL of p-NP (1 mM) were added into a quartz cuvette for recycling test. To investigate the reduction of p-NP by other iron minerals, we prepared the stock suspensions by mixing with $NaBH_4$ (100 mM) in anaerobic chamber. The reduction of p-NP was performed using 10 mg/L iron minerals, 50 mM $NaBH_4$, and 0.1 mM p-NP in an oxygen environment.

2.4. HPLC and Fe measurement

The concentration of p-NP and p-AP in aqueous solution was measured by high performance liquid chromatography (HPLC) (Waters) equipped with a C18 packed column (Waters) and UV detector. After finishing each reduction experiment, the aqueous sample (around 2.7 mL) was collected from the cuvette and 1.7 mL of sample was filtered by 0.2-μm membrane filter for HPLC and Fe measurement. Mobile phase was a mixture of 50% deionized water (DIW), 50%

acetonitrile, and 1% CH_3COOH. The p-NP and p-AP were measured at a flow rate of 1.0 mL min^{-1} at wavelengths of 317 nm and 273 nm, respectively.

Fe loss during the reduction of p-NP and magnetic separation was measured by Ferrozine method using a UV-vis spectrophotometer (UV-1205, SHIMADZU) at the wavelength of 562 nm [25]. The membrane-filtered sample was used for measurement of dissolved Fe and 1 mL of aqueous solution remained from magnetic separation was transferred to 1 mL of 6 M HCl for measurement of total Fe by adding 10% hydroxylamine solution [26]. No significant amount of Fe was detected in membrane-filtered sample in most cases, indicating that dissolved Fe during the reduction of p-NP can be negligible in this study due to the high pH (>10) of $NaBH_4$ solution.

2.5. Surface characterization

The changes in particle morphology of NZVI were identified by transmission electron microscope (TEM, JEM-2100, JEOL). We prepared a variety of NZVI particles; 1) initial NZVI (oxygen free environment), 2) reacted with $NaBH_4$ (100 mM, oxygen free environment), 3) after the reduction of p-NP with $NaBH_4$ (five recycling, oxygen environment), and 4) without $NaBH_4$ (one reaction, oxygen environment). After the reaction, the samples were transferred to anaerobic chamber and washed by deaerated ethanol twice. We put one droplet of the diluted suspension on Cu TEM grids and analyzed the samples by TEM at an acceleration voltage of 200 kV. X-ray photoelectron spectroscopy (XPS) was conducted to identify the redox states of Fe on NZVI surface using the samples prepared for TEM. The samples were dried after the reactions in anaerobic chamber for 24 h and carefully packed on XPS sampling template. Then, they were transferred to the vials containing deaerated ethanol to avoid the oxidation of NZVI during the installation of XPS template. XPS analysis was carried out using a Sigma Probe (Thermo) with a Al kα X-ray (1486.7 eV). Surface charging effects were corrected with C 1s

peak at 285 eV as a reference. We used Shirley baseline and a Gaussian-Lorentzian peak shape for fitting the data. NZVI with/without $NaBH_4$ were also identified by X-ray diffraction (XRD) (D8, BRUKER). The NZVI suspensions prepared in ethanol were used for XRD analysis. The suspension were transferred to XRD holder and dried for 2 h in anaerobic chamber. Then, the dried samples were treated with 1:1 (v:v) glycerol solution to avoid the oxidation of Fe(0) during the analysis of XRD [20]. Attenuated total reflectance-Fourier transform infrared (ATR-FTIR) spectra were recorded between 4000 and 650 cm^{-1} on a Nicolet iS50 FT-IR spectrometer system (Thermo Scientific Inc.) equipped with a MCT/A detector cooled with liquid N_2. A nine-reflection diamond ATR accessory was used for acquiring spectra of the samples. One droplet of p-NP (10 mM) was first put onto the diamond ATR crystal, and then followed by adding one droplet of NZVI suspension (10 g/L) prepared in $NaBH_4$ (100 mM). ATR-FTIR spectra were recorded at room temperature at a 4 cm^{-1} resolution by averaging 100 scans.

2.6. Computational details

We performed DFT calculations to understand the reduction pathway of p-NP using the Vienna Ab-initio Software Package (VASP) program [27] with the choice of Perdew-Burke-Emzerhof (PBE) exchange-correlation functional [28]. According to the results obtained from our experiments and other references [29], the outer shell of NZVI seemed to be covered by iron oxides especially magnetite form. We thus used a slab model of magnetite that is a (4 × 4) Fe_3O_4 (111) surface where bottom 1/3 layer is fixed at a lattice point to assume it as the bulk, whereas the upper layers were allowed to be relaxed (Fig. S1). To avoid the interaction between slab models over the periodic boundary cell, we included a vacuum slab of ~ 20A along the c-direction of our simulation cell. Due to the limited computational cost as well as the large enough simulation cell of 12 Å × 12 Å × 25 Å, only Gamma point is sampled in the reciprocal space, and an energy cutoff of 450 eV is used for the plane wave basis set.

3. Results and discussion

3.1. Effect of $NaBH_4$ on NZVI properties.

In the absence of $NaBH_4$, TEM images of NZVI showed chain-like aggregates consisting of spherical shape of particles (60−100 nm) (Fig. 1a). Each individual particle was covered by 2.5–3.5 nm of iron oxide shell (Fig. 1b). It should be noted that the NZVI particles became much smaller (15-40 nm) by addition of $NaBH_4$ (100 mM) (Fig. 1c), but kept the same morphology (i.e., spherical shape of particles with 2.5–3.5 nm of iron oxide shell) (Fig. 1d). The formation of smaller nanoparticles by $NaBH_4$ could be caused by oxidative dissolution of NZVI or by chemical etching reaction on iron oxide layer. It is well-known that adsorption of borohydride on the particle surface can negatively shift in the redox potential of metallic nanoparticle, which can proceed oxidative dissolution of metals due to high susceptibility toward oxidation by oxygen [30]. Then the dissolved metal ions can be also reduced by $NaBH_4$ to form new nanoparticles once the oxygen level falls below a critical value, as previously observed by silver nanoparticle [30]. In the present work, the formation of smaller nanoparticles upon $NaBH_4$ addition was, however, observed in oxygen-free environment, ruling out the role of oxidative dissolution. Consequently, we rather suspect that chemical etching reaction may occur at magnetite surfaces which can lead to the disintegration of microsized magnetite into nanosized magnetite following further by a magnetism-induced self-assembly of magnetite [31]. This mechanism seems to happen here, as magnetite is supposed to be present in the oxidized layer of NZVI. After forming of smaller NZVI particles by addition of $NaBH_4$ (Fig. S2a and 2b), the particles are aggregated each other again, resulting in formation of flower-like aggregates (Fig. S2c). In addition, XRD data of initial NZVI particles (Fig. 1e) revealed the presence of peaks of α-Fe (44.6° 2θ), magnetite (57.0° 2θ), and broad peak of iron oxides (hematite (33.5° 2θ) and magnetite (35.3° 2θ)). Interestingly, the broad peak of iron oxides

continuously decreased as the concentration of $NaBH_4$ increased from 1 to 100 mM (Fig. 1e), 218 indicating that characteristic of α-Fe seems to be stronger at higher $NaBH_4$ concentration due 219 probably to the formation of many smaller NZVI particles as shown in TEM images, or the 220 reduction of oxide coatings to α-Fe by $NaBH_4$. XPS analysis was conducted to confirm the 221 reduction of NZVI surfaces by addition of $NaBH_4$ (Fig. 2). The XPS spectra for Fe($2p_{3/2}$) were 222 composed of four different peaks at 706.4–706.6, 709.2–709.7, 710.9–711.5, and 712.7–713.1 223 eV which were assigned to the binding energies for Fe^0 (706.4 eV), Fe^{2+}-O (709–709.5 eV), 224 and Fe^{3+}-O (711–714 eV), respectively [20]. The proportion of Fe^{3+} on the NZVI surface 225 decreased from 68.1 to 57.4% upon $NaBH_4$ addition, while increasing in the proportion of Fe^{2+} 226 (26.9 → 32.0%) and Fe^0 (4.9 → 10.5%) was observed (Fig. 2a and b). We also observed the 227 presence of two peaks at 187.9 and 191.7 eV (inset in Fig. 2b), which could be assigned to B in Fe^0-B and BO_2^-, respectively [31]. The results from TEM, XRD, and XPS confirmed that $NaBH_4$ can effectively interact with NZVI leading to the disintegration of NZVI into much smaller particles and reduction of outermost surfaces to Fe^{2+} and/or Fe^0-B.

3.2. Reduction of p-NP by NZVI with $NaBH_4$

The concentration of $NaBH_4$ (1-100 mM) used in this study was not able to reduce p-NP. On 234 the contrary, addition of p-NP into NZVI-$NaBH_4$ suspension showed the color change from 235 yellow to colorless in 30 min (Fig. 3a), indicating a complete reduction of p-NP. Fig. S3 shows 236 UV-vis spectra during the reduction. The initial absorption peak of p-NP is shifted from 317 to 237 400 nm after addition of $NaBH_4$ (pH = 10.4) due to the formation of *p*-nitrophenolate ions [10]. 238 The continuous decrease in absorption peak of the ionized p-NP at 400 nm was observed with 239 formation of new peak at 300 nm, which is known to be p-AP [14,32]. We noticed fluctuation 240 of the baseline (Fig. S3) due to H_2 production from the $NaBH_4$ solution ($BH_3 + 3H_2O \rightarrow H_3BO_2$

+ $3H_2$) and its enhanced production by catalyst (i.e., nanoscale zero-valent iron). Indeed, a vigorous production of H_2 bubbles was observed during the reaction. However, a complete removal of p-NP was clearly observed at an identical baseline (Fig. 3b) and HPLC analysis confirmed the 98% of p-NP removal with 97% of p-AP production after 30 min (Fig. 3c, inset). The decrease in absorbance at 400 nm (Fig. 3c) was also observed due to the initial mixing of p-NP in NZVI suspension. Because the complete reduction of p-NP to p-AP needs six electrons from NZVI ($HOC_6H_4NO_2 + 6e^- + 6H^+ \rightarrow HOC_6H_4NH_2 + 2H_2O$), 0.1 mM p-NP cannot be completely reduced by 0.065 mM NZVI. Indeed, 2.8 times higher NZVI concentration (0.18 mM) without $NaBH_4$ was able to reduce only 0.01 mM p-NP in O_2-free environment (Fig. S4). The results suggest that addition of $NaBH_4$ into NZVI suspension can overwhelm theoretical reduction capacity of NZVI toward p-NP. The reduction of p-NP by NZVI was able to be described by pseudo-first-order kinetic model ($R^2 = 0.98$), as previously reported for other metallic noble catalysts (Fig. 3c) [9,10,32]. The rate constants with $NaBH_4$ in an oxygen environment ($k_{obs\text{-}p\text{-}NP} = 3.1 \times 10^{-1}$ min^{-1}) were approximately three orders of magnitude higher than that without $NaBH_4$ in an oxygen free environment ($k_{obs\text{-}p\text{-}NP} = 7.1 \times 10^{-4}$ min^{-1}), indicating that addition of $NaBH_4$ can significantly enhance the reduction rate of p-NP to p-AP by NZVI even in oxygen environments.

Interaction of target molecules with NZVI surfaces is a prerequisite to induce electron transfer, leading to reductive transformation of the sorbed molecules. To investigate the surface mediated reactions, *in-situ* ATR-FTIR analysis was carried out by recording the spectra of NZVI reacted with $NaBH_4$ and p-NP (Fig. 4). It is note-worthy that NO_2 stretch band at 1114 cm^{-1}, CH/OH bend at 1171 cm^{-1}, and CC/C-H bend at 1295 cm^{-1} appeared at the initial stage (2 min), indicating that p-NP can be initially adsorbed on NZVI surfaces through both NO_2 and oxygen of the phenolate group [33]. However, these three main peaks continuously decreased as reaction proceeded and finally disappeared after 78 min with increase of peaks at 1240 cm^{-1}

(C-NH_2 stretch) [34]. This indicates that p-AP may be formed in the vicinity of NZVI surfaces, before being released into solution. The latter has been confirmed by checking the mass balance in aqueous solution, where conversion yield of p-NP to p-AP lied at around 95%.

3.3. Recycling tests and effect of $NaBH_4$ concentration

The stability and recyclability of NZVI with $NaBH_4$ was evaluated by monitoring the reactivity of NZVI during five times of reaction cycles (Fig. 5). UV-vis analysis showed complete reduction of p-NP in 30 min during four reaction cycles (Fig. 5a). HPLC analysis also showed the removal of p-NP over 98% with the production of p-AP over 92% (Fig. 5b), thereby underscoring the excellent stability of NZVI reactivity. The very little loss of p-AP production may be caused by the adsorption of p-AP on NZVI surfaces, as it is expected based on FTIR data. Similarly to previous studies showing a continuous decrease in catalytic activity with increase in number of recycling [10,29], the reduction extent slightly decreased to 93% of p- NP removal (*vs* 89% of p-AP production) over 5 cycles (Fig. 5b). This slight decrease in reduction efficiency may be attributed to the loss of NZVI particles during the magnetic separation. Doong's group has also reported that the catalytic activity of Au-magnetite catalyst continued to decrease due to the loss of nanoparticles during the separation process [7,10]. Because we used an extremely small amount of NZVI (0.065 mM) for the reaction, even small loss of NZVI during the magnetic separation can significantly influence the next reaction performance. Indeed, we observed a small loss of Fe (5-8 μM) during the magnetic separation process at each cycle (Fig. 6a). A relationship between the pseudo-first-order kinetic rate constant after the second cycle and Fe remained at each cycle was properly fitted by a linear regression (R^2 = 0.99) (Fig. 6b), confirming that Fe loss during the recycling test was a primary reason for decrease in NZVI reactivity. The enhancement of reduction rate constant observed between the first and the second cycle may be attributed to the higher ratio of $NaBH_4$: NZVI

during washing process. We prepared the NZVI stock suspension (1.95 mM) in 100 mM of $NaBH_4$ (51:1 molar ratio of $NaBH_4$:NZVI), then 0.1 mL of stock suspension transferred to the cuvette (0.065 mM of NZVI) for the first reduction cycle of p-NP. After second cycle, the molar ratio of $NaBH_4$:NZVI increased to 1538:1 by washing with 100 mM of $NaBH_4$, which can significantly enhance the reaction between $NaBH_4$ and NZVI. The rate constant at second cycle after washing by 10 mM $NaBH_4$ ($k_{obs\text{-}p\text{-}NP}$ = 3.8 × 10^{-1} min^{-1}) was 2.4 times lower than that by 100 mM $NaBH_4$ ($k_{obs\text{-}p\text{-}NP}$ = 9.1 × 10^{-1} min^{-1}) (Fig. 6b), indicating the effect of $NaBH_4$ concentration on NZVI reactivity. To investigate the effect of $NaBH_4$ concentration, lower $NaBH_4$ concentrations (5 and 25 mM) for p-NP reduction were investigated (Fig. S5). p-NP reduction in 25 mM $NaBH_4$ showed similar reduction kinetics as for 50 mM $NaBH_4$ at first cycle, but lower reduction kinetics at second cycle. This may be caused by the prevention of NZVI oxidation at higher $NaBH_4$ concentration in oxygen environments. In the case of 5 mM $NaBH_4$, only 39% of p-NP was reduced in 60 min, which confirms that higher concentration of $NaBH_4$ can positively act not only for enhancement of catalytic activity but also for effective preservation of NZVI during the reduction of p-NP to p-AP.

TEM, XRD, and XPS analyses were carried out to compare the NZVI particles after five reaction cycles with $NaBH_4$ and after one reaction cycle without $NaBH_4$ (Fig. 7 and Fig. 2d). TEM images showed that small NZVI particles were preserved even after five recycling in an oxygen environment (Fig. 7a and b), and XRD diffractogram was very similar to that of NZVI in 100 mM $NaBH_4$ before the reaction (Fig. 7e). The result from XPS also revealed that the surface of NZVI was composed of approximately 7.2% of Fe^0, 36.0% of Fe^{2+}, and 56.8% of Fe^{3+} (Fig. 2c). This indicates that the proportion of Fe^{3+} was very similar to that of NZVI in 100 mM $NaBH_4$ (Fig. 2b), but that of Fe^{2+} slightly increased (32.0 → 36.0%) as well as for that of Fe^0 (10.5 → 7.2%). The slight increase in Fe^{2+} after the five recycling may be induced by the continuous electron transferring from Fe^0 to p-NP, which can be re-reduced to Fe^0-B by $NaBH_4$

as shown in Fig. 2b. In contrast, NZVI sample without $NaBH_4$ (right after first reaction) showed the presence of non-uniform platy particles (20−40 nm) and needle-shaped particles (>100 nm) in TEM images (Fig. 7c and d). These shapes may correspond to magnetite and lepidocrocite, which have been previously observed for the oxidation of NZVI by carbon tetrachloride and oxygenated water, respectively [20,35]. Consistently, XRD diffractogram revealed the presence of magnetite (30, 35.3, 57.0, and 62.3° 2θ) and lepidocrocite (27.1, 43.5 and 46.9° 2θ) (Fig. 7e) and XPS spectra showed a significant increase in proportion of Fe^{3+} (72%) with a disappearance of peak for Fe^0 (Fig. 2d). Therefore, these results confirm the rapid oxidation of NZVI to Fe- oxides or Fe-oxyhydroxides during the reduction of p-NP without $NaBH_4$ in oxygen environments.

3.4. Borohydride-induced catalytic p-NP reduction on magnetite surface (experimental and theoretical studies).

As an attempt to elucidate the borohydride-induced catalytic p-NP reduction mechanism, the ability of four iron oxy(hydr)oxides, suspected to coat the spherical NZVI particles, to reduce p-NP in the presence of $NaBH_4$ was investigated (Fig. 8). First, a slight decrease in absorbance at 400 nm and its rebound to initial concentration of p-NP was observed in maghemite, hematite, and goethite suspensions as similar to p-NP alone, due to the initial mixing effect of p-NP solution (see experimental section). HPLC analysis confirmed that the removal of p-NP were 0, 2, and 8% by maghemite, hematite, and goethite, respectively, while no p-AP was detected, suggesting that the p-NP decay may be caused by its adsorption on the surface of hematite and goethite. In contrast, a significant decrease in p-NP absorbance was observed in magnetite suspension, resulting in 72% of p-NP reduction with 65% of p-AP production. However, we observed a little effect on the reduction of p-NP by magnetite at low $NaBH_4$ concentration (1-10 mM). It is worth noting that only magnetite showed the formation of H_2

bubbles during the reduction of p-NP, corroborating the occurrence of a chemical reaction. This catalytic activity of magnetite may be attributed to the structural modifications occurred on magnetite surfaces, such as generation of smaller crystals and formation of Fe^0-B amorphous alloy [31] and/or the catalytic activity of magnetite for p-NP induced by the presence of $NaBH_4$. The former has been already shown to exhibit a catalytic activity such as dehydrogenation of ethanol [36].

To investigate the catalytic activity of magnetite for p-NP induced by the presence of $NaBH_4$, DFT calculations were performed (Fig. 9 and Table S1). Although the existence of p-nitrophenolate anion was observed in our experimental conditions, we used a protonated form of the phenol group for DFT calculations to maintain the simulation cell neutrality without including explicit solvent molecules. Considering that the reaction center locates at the opposite functional group of NO_2, we expect that the deprotonation of the phenol group will barely influence the relative energetics. We note that tetrahedral Fe^{3+} sites are exposed at the magnetite (111) surface, which has been often investigated as a rational structure of magnetite (111) for catalytic purposes in both theoretical and experimental studies [37-40]. In our systems, the adsorption energy of p-NP on top of the tetrahedral Fe^{3+} site is also calculated as favorable (ΔE_{ads} = -0.38 eV (Table S2)), which is followed by the first nucleophilic attack of hydride (H^-) of $NaBH_4$ to the nitrogen atom with the low electronegativity, yielding NHO_2^- group ($\Delta E_{hyd\text{-}trs(1st)}$ = -0.91 eV). Then, the NHO_2^- group is dehydroxylated into NO group to form *p*-nitrosophenol ($\Delta E_{dehydr(1st)}$ = -0.46 eV downhill), which is further converted into NHO^- group by the second hydride transfer from $NaBH_4$ ($\Delta E_{hyd\text{-}trs(2nd)}$ = -1.95 eV). The strong Brønsted acidity of NHO^- group induces hydrolysis to form NH_2O group, producing p-hydroxyaminophenol (ΔE_{hydrol} = 0.11 eV). The third hydride transfer from $NaBH_4$ further reduces the NH_2O group to NH_3O^- group ($\Delta E_{hyd\text{-}trs(2nd)}$ = -0.39 eV), which is followed by the second dehyroxylation, eventually yielding the final product of p-AP ($\Delta E_{dehydr(2nd)}$ = -2.11 eV).

We note that our overall mechanism ($HOC_6H_4NO_2 + 3NaBH_4 + H_2O \rightarrow HOC_6H_4NH_2 + 3NaOH + 3BH_3$) is mediated by the intermediate species of *p*-nitrosophenol and *p*-hydroxyaminophenol, which is consistent with previous studies (Fig. 10) [12, 41, 42]. In addition, once BH_3 is formed, it can be further oxidized to H_3BO_3 ($BH_3 + 3H_2O \rightarrow H_3BO_3 + 3H_2$) by water in alkaline aqueous environment [43]. Therefore, we propose the entire reaction pathway for $NaBH_4$ induced p-NP reduction on magnetite surface by adding the oxidation of BH_3 ($HOC_6H_4NO_2 + 3NaBH_4 + 10H_2O \rightarrow HOC_6H_4NH_2 + 3NaOH + 3H_3BO_3 + 9H_2$). To identify the role of magnetite surface, we compared the energetics for p-NP to p-AP reduction pathway when the reaction proceeds without magnetite surface (Fig. 9 and Table S2). We found that the first and second hydride transfer steps become energetically disfavored ($\Delta E_{hyd\text{-}trs(1st)}$ = +1.01 eV and $\Delta E_{hyd\text{-}trs(2nd)}$ = +0.55 eV), indicating that reduction of p-NP cannot occur in $NaBH_4$ solution without magnetite, as it was experimentally observed. The experimental results and DFT calculations suggest that the combination of disintegration of NZVI into smaller size, formation of Fe^0-B, and catalytic activity of magnetite may be responsible of the enhanced reduction of p-NP to p-AP.

4. Conclusions

Although NZVI technologies have been extensively studied for reduction of environmental contaminants, the rapid passivation of NZVI surface limits its application in ambient environments (21% O_2 condition). Herein, we have demonstrated that the $NaBH_4$ enhanced significantly the reactivity of NZVI in oxygen environments. Our surface and solution characterization and DFT calculations revealed that the $NaBH_4$ acts through one or combination of the following mechanisms: (i) disintegration of NZVI into much smaller particles increasing reactive surface available for NP reduction, (ii) reaction with oxides coatings in the NZVI shell leading to the formation of new surface sites with a high reductive ability and (iii) hydrolysis

of p-NP to p-AP by interaction between magnetite shell and $NaBH_4$. Moreover, the reduction of p-NP to p-AP in an oxygen environment was significantly enhanced by NZVI with $NaBH_4$ compared to NZVI without $NaBH_4$ in an oxygen-free environment. Therefore, NZVI-$NaBH_4$ system can be supposed to preserve the NZVI reactivity in contaminated systems containing naturally occurring oxidant species (e.g. O_2 and/or nitrate). The high conversion efficiency, and good reactivity/reusability are likely comparable with the widely used noble metallic catalysts (e.g., Au, Ag, and Pt). Although $NaBH_4$ should be carefully handled due to its production of flammable and explosive H_2 gas during the reaction with water or moist air [44], the new findings obtained from NZVI, produced by easy and cheap methods, can provide a novel possibility for mass production of p-AP from p-NP in NZVI-$NaBH_4$ system. These results can also help researchers and technicians for the development of novel NZVI technologies, which can apply to the reductive degradation of environmental contaminants in oxygen environments.

Acknowledgements

The authors would like to thank the "Région Bretagne" for financial support (Contract SAD-ReSolEau (8256)). The authors thank Dr. M. Pasturel and Dr. V. Dorcet for XRD and TEM analyses, respectively.

References

[1] ATSDR. Toxicological profile for nitrophenols: 2-Nitrophenol and 4-nitrophenol; Agency for Toxic Substances and Disease Registry, Public Health Service, 1992.

[2] HSDB. 4-Nitrophenol (CASRN: 100-02-7); Hazardous Substances Data Bank, U.S. National Library of Medicine, National Institutes of Health, Department of Health & Human Services, 1999.

[3] EPA. *Water quality criteria*; Environmental Protection Agency: Washington DC, 1976. 416

[4] A. Gangula, R. Podila, M. Ramakrishna, L. Karanam, C. Janardhana, A.M. Rao, Langmuir 27 (2011) 15268–15274.

[5] S. Wunder, F. Polzer, Y. Lu, Y. Mei, M. Ballauff, J. Phys. Chem. C 114 (2010) 8814–8820.

[6] S. Jana, S.K. Ghosh, S. Nath, S. Pande, S. Praharaj, S. Panigrahi, S. Basu, T. Endo, T. Pal, Appl. Catal. A 313 (2006) 41–48.

[7] F-H. Lin, R-A. Doong, Appl. Catal. A 486 (2014) 32-41.

[8] K.S. Shin, Y.K. Cho, J.-Y. Choi, K. Kim, Appl. Catal. A 413–414 (2012) 170–175. 423

[9] J. Li, C.Y. Liu, Y. Liu, J. Mater. Chem. 22 (2012) 8426–8430.

[10] F.H. Lin, R.A. Doong, J. Phys. Chem. C 115 (2011) 6591–6598.

[11] T.A. Aditya, A. Pal, T. Pal, Chem. Commun. 51 (2015) 9410–9431.

[12] S. Gu, S. Wunder, Y. Lu, M. Ballauff, J. Phys. Chem. C 118 (2014) 18618–18625. 427

[13] R. Fenger, E. Fertitta, H. Kirmse, A.F. Thunemann, K. Rademann, Phys. Chem. Chem. Phys. 14 (2012) 9343–9349.

[14] X. Kong, Z. Sun, M. Chen, C. Chen, Q. Chen, Energy Environ. Sci. 6 (2013) 3260–3266.

[15] N. Pradhan, A. Pal, T. Pal, Colloids Surf. A 196 (2002) 247–257.

[16] A.L. Roberts, L.A. Totten, W.A. Arnold, D.R. Burris, T.J. Campbell, Environ. Sci. Technol. 30 (1996) 2654–2659.

[17] M.J. Alowitz, M.M. Scherer, Environ. Sci. Technol. 36 (2002) 299−306.

[18] S. Bae, W. Lee, Appl. Catal. B: Environ. 96 (2010) 10−17.

[19] Y. Xie, D.M. Cwiertny, Environ. Sci. Technol. 46 (2012) 8365−8373.

[20] S. Bae, W. Lee, Environ. Sci. Technol. 48 (2014) 2368−2376.

[21] Y. Shin, S. Bae, W. Lee, Adv. Environ. Res. 2 (2013) 167–177.

[22] S. Bae, K. Hanna, Environ. Sci. Technol. 49 (2015) 10536−10543.

[23] M. Usman, M. Abdelmoula, P. Faure, C. Ruby, K. Hanna, Geoderma 197 (2013) 9–16.

[24] M. Usman, M. Abdelmoula, K. Hanna., B. Grégoire, P. Faure, C. Ruby, J. Solid State Chem. 194 (2012) 328–335.

[25] L.L. Stookey, Anal. Chem. 42 (1970) 779–781.

[26] S. Bae, D. Kim, W. Lee, Appl. Catal. B: Environ. 134-135 (2013) 93–102.

[27] G. Kresse, J. Furthmuller, Phys. Rev. B 54 (1996) 11169–11186.

[28] J.P. Perdew, K. Burke, M. Ernzerhof, Phy. Rev. Lett. 77 (1996) 3865–3868.

[29] F. Sun, K.A. Osseo-Asare, Y. Chen, B.A. Dempsey, J. Hazard. Mater. 196 (2011) 311–317.

[30] T. Pal, T.K. Sau, N.R. Jana, Langmuir 13 (1997) 1481–1485.

[31] Q. Hua, W. Huang, J. Mater. Chem. 18 (2008) 4286–4290.

[32] M. An, J. Cui, L. Wang, J. Phys. Chem. C118 (2014) 3062–3068.

[33] A. Perry, H.J. Son, J.S. Cordova, L.G. Smith, A.S. Biris, J. Colloid Interface Sci. 342 (2010) 311–319.

[34] D.A. Perry, J.S. Cordova, L.G. Smith, H.J. Son, A.S. Biris, Vib. Spectrosc. 55 (2011) 77–84.

[35] A. Liu, J. Liu, B. Pan, W-X. Zhang, RSC Adv. 4 (2014) 57377–57382.

[36] B. Rajesh, N. Sasirekha, Y.W. Chen, S.P. Lee, Ind. Eng. Chem. Res. 46 (2007) 2034–2041.

[37] C. Lemire, R. Meyer, V.E. Henrich, Sh. Shaikhutdinov, H.-J. Freund, Surf. Sci. 572 (2004) 103–114.

[38] K. Rim, D. Eom, S. Chan, M. Stephanopoulos, G.W. Flynn, X. Wen, E.R. Batista, J. Am. Chem. Soc. 134 (2012) 18979–18985.

[39] A. Barbieri, W. Weiss, M.A. Hove, G.A. Somorjai, Surf. Sci. 302 (1994) 259–279.

[40] M. Ritter, W. Weiss, Surf. Sci. 432 (1999) 81–94.

[41] S. Pandey, S.B. Mishra, Carbohydr. Polym. 113 (2014) 525–531.

[42] R. Konig, M. Schwarze, R. Schomacker, C. Strubenrauch, Catalyst 4 (2014) 256–275. 466

[43] R.E. Davis, E. Bromels, C.L. Kibby, J. Am. Chem. Soc. 84 (1962) 885–892.

[44] New Jersey Department of Health and Senior Services Website; http://nj.gov/health/eoh/rtkweb/documents/fs/2063.pdf

Fig. 1. TEM images showing the NZVI particles without $NaBH_4$ (a and b) and with $NaBH_4$ (c and d) and (e) XRD patterns of NZVI in different concentrations of $NaBH_4$.

Fig. 2. XPS spectra for the narrow scan of $Fe(2P_{3/2})$ on the surface of (a) initial NZVI, (b) NZVI reacted with $NaBH_4$ (Inset: narrow scan of B(1s)), (c) NZVI after five reaction cycles with p-NP in the presence of $NaBH_4$, and (d) NZVI after one reaction cycle with p-NP in the absence of $NaBH_4$.

Fig. 3. (a) Color change of p-NP suspension during the reaction and NZVI separation by magnetism. (b) Background compensated UV-vis spectral change in p-NP (0.1 mM) in the presence of NZVI (3.5 mg/L, 0.065 mM). (c) Concentration changes of p-NP analyzed by UV-vis data and the conversion efficiency after finishing the reaction (inset). The pH is highly alkaline (~11) due to the addition of $NaBH_4$ solution.

Fig. 4. ATR-FTIR spectra during the reduction of p-NP (10 mM) by NZVI (10 g/L) with $NaBH_4$ (100 mM).

Fig. 5. (a) Reduction kinetics of p-NP (0.1 mM) by NZVI (3.5 mg/L, 0.065 mM) during the recycling test and (b) the conversion efficiency after finishing each cycle. The pH is highly alkaline (~11) due to the addition of $NaBH_4$ solution.

Fig. 6. (a) Fe loss during the separation process and (b) change in $k_{obs\text{-}p\text{-}NP}$ with respect to the Fe(0) concentration remained at each cycle.

Fig. 7. TEM images showing the NZVI particles after five reaction cycles with p-NP in the presence of $NaBH_4$ (a and b) and after one reaction cycle in the absence of $NaBH_4$ (c and d) and (e) their XRD patterns

Fig. 8. Removal kinetics of p-NP by Fe minerals (maghemite, hematite, goethite, and magnetite) and (b) their conversion efficiencies

Fig. 9. Hydrolysis mechanism of p-NP to p-AP on magnetite surface based on the DFT calculations. Black lines show the energetics with magnetite (111) surface, while the energetics without magnetite surface are shown as grey lines.

Fig. 10. Reaction mechanism proposed by this study for p-NP reduction to p-AP on magnetite surface by $NaBH_4$.

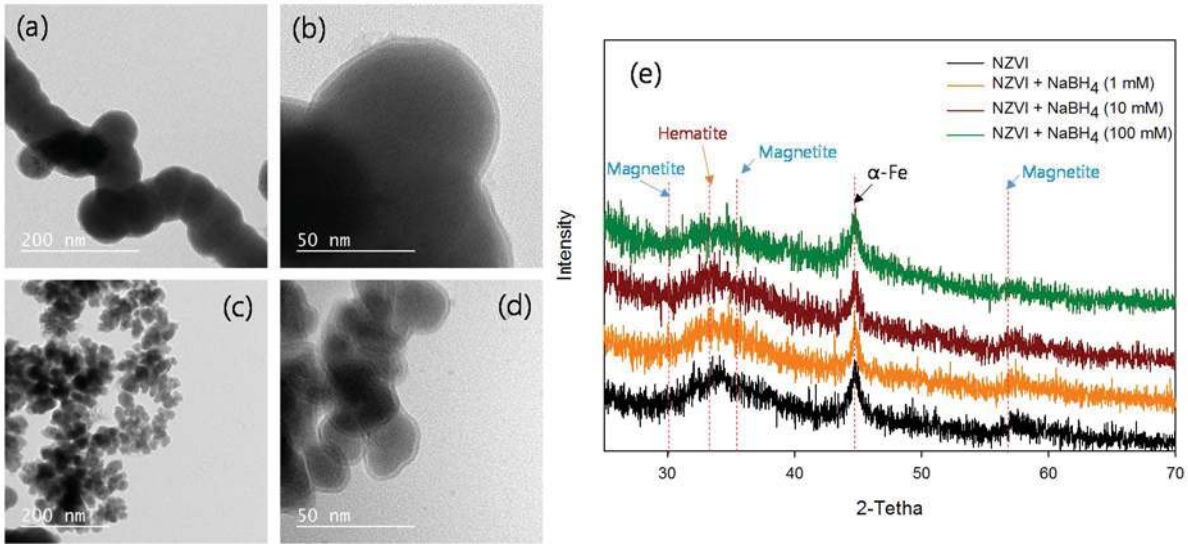

Fig. 1

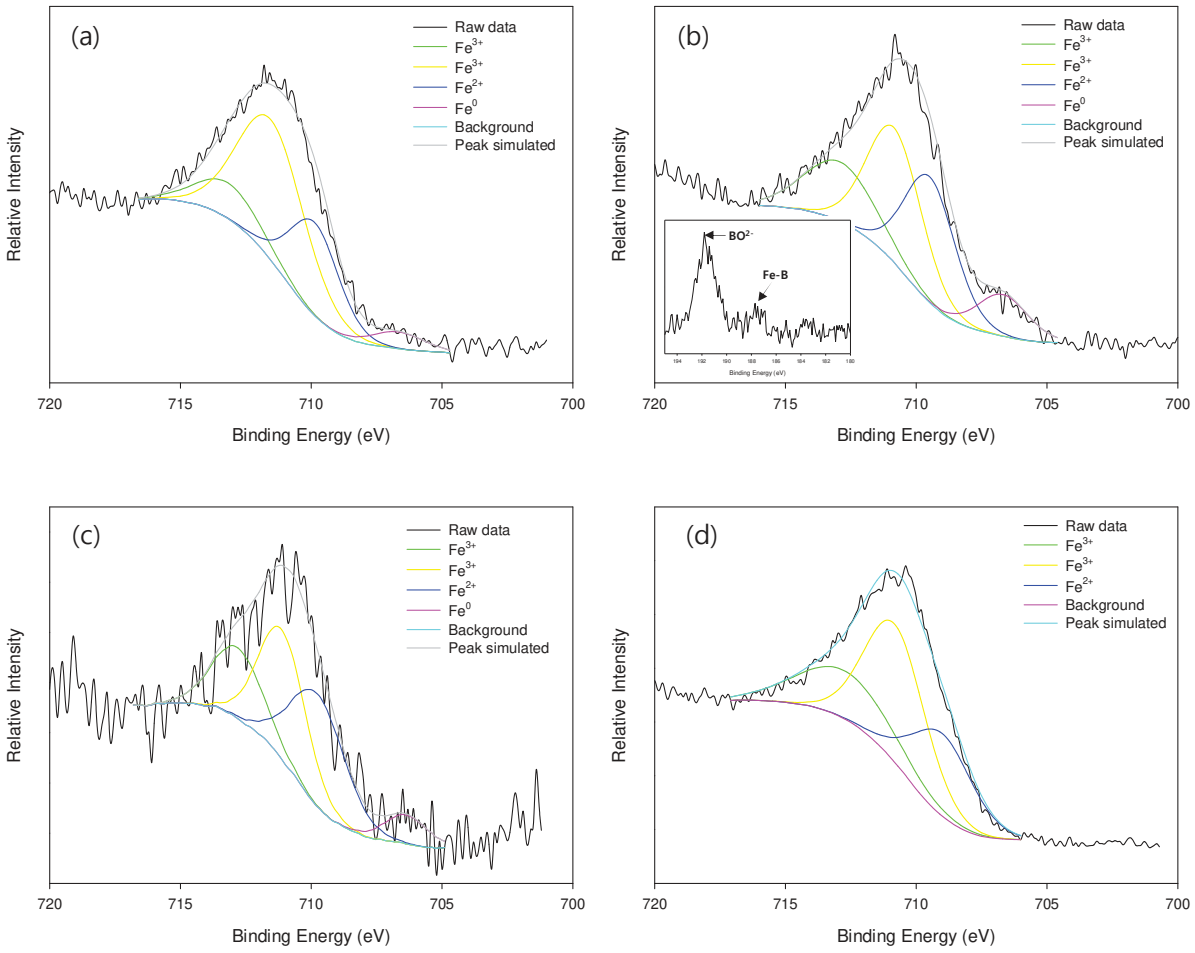

Fig. 2

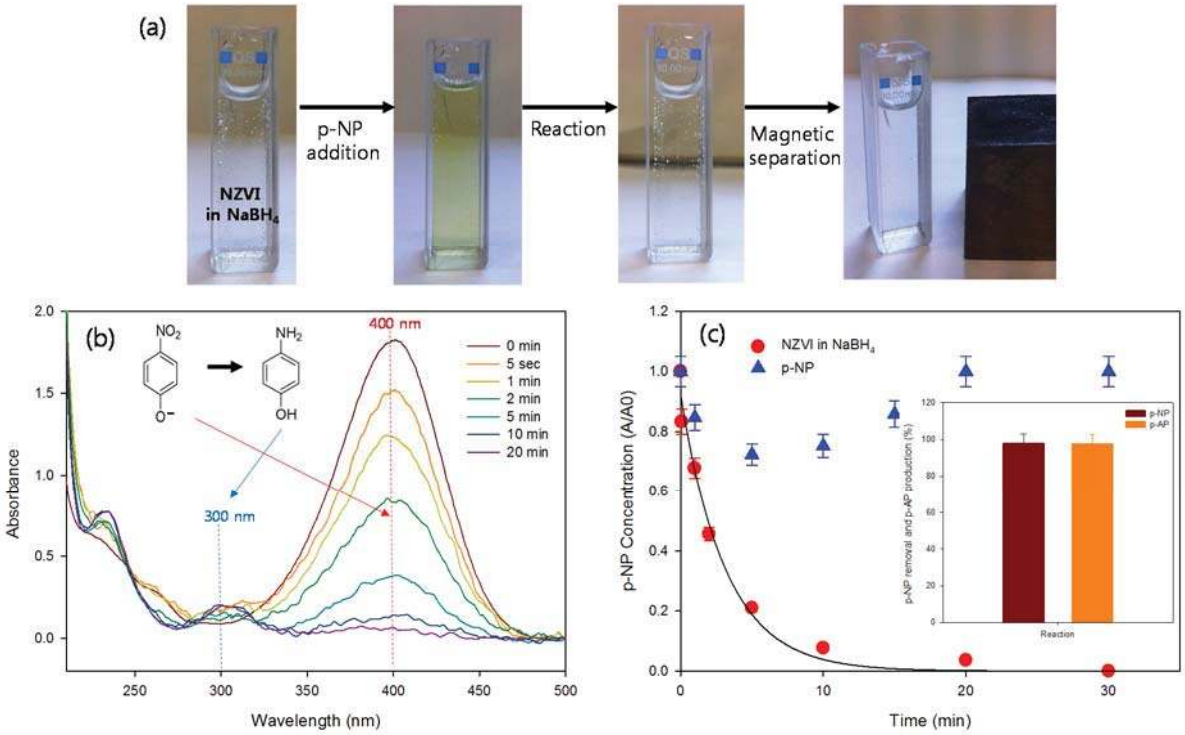

Fig. 3

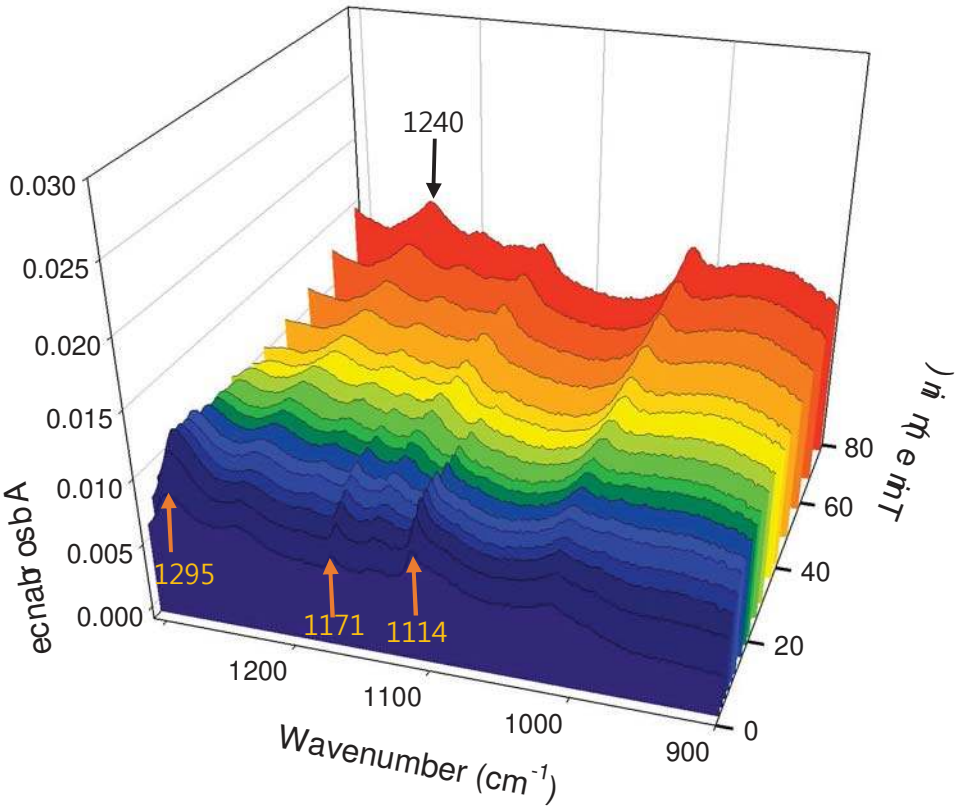

Fig. 4

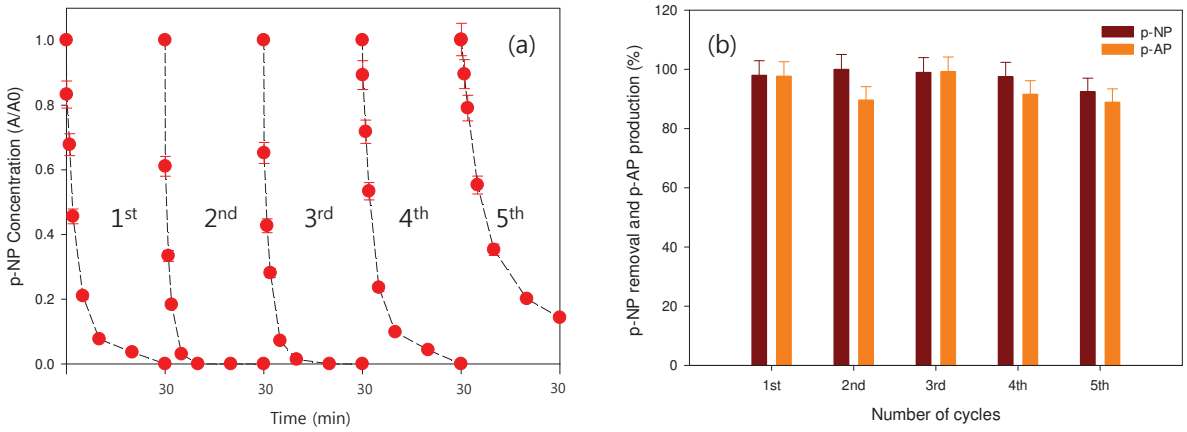

Fig. 5

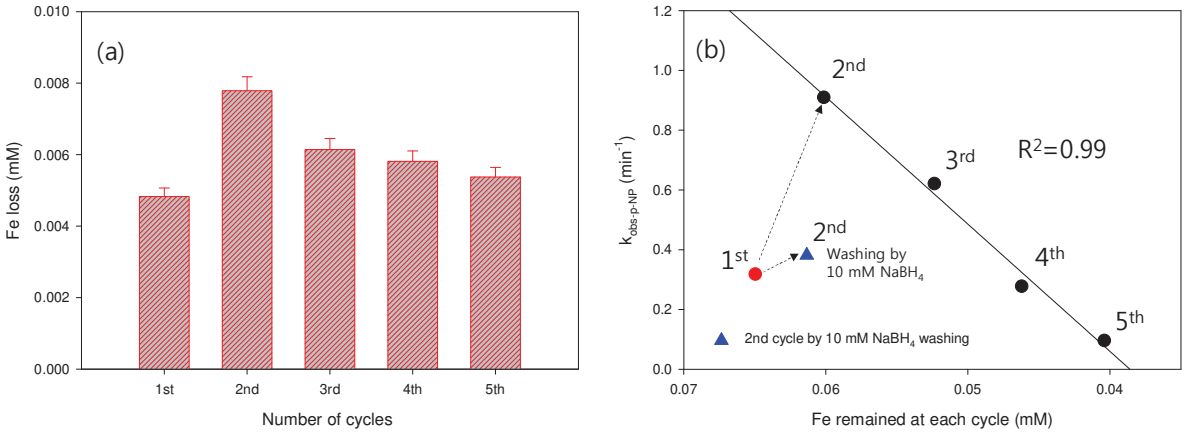

Fig. 6

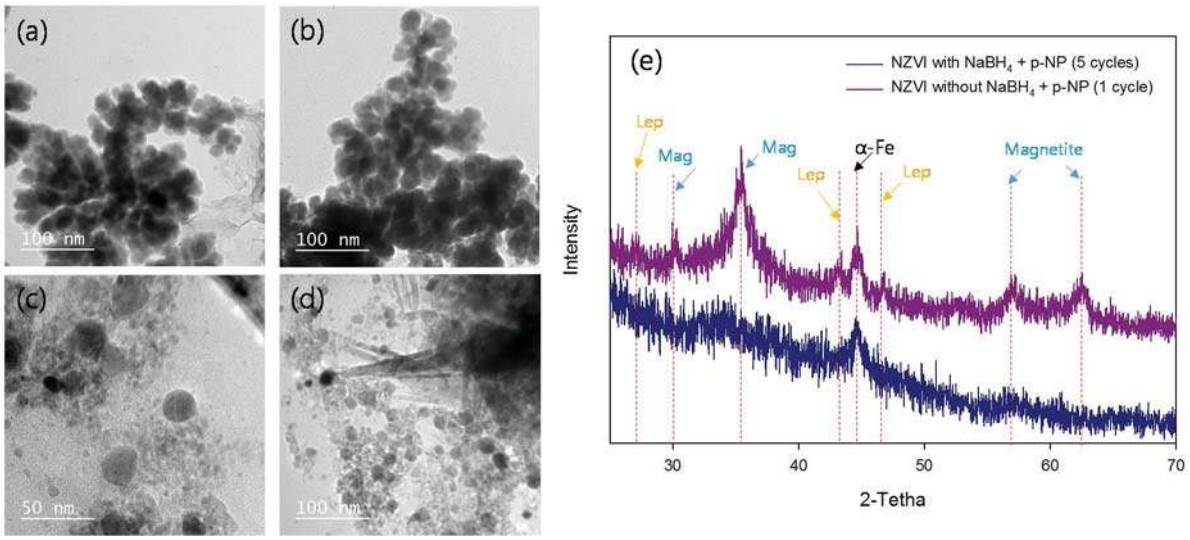

Fig. 7

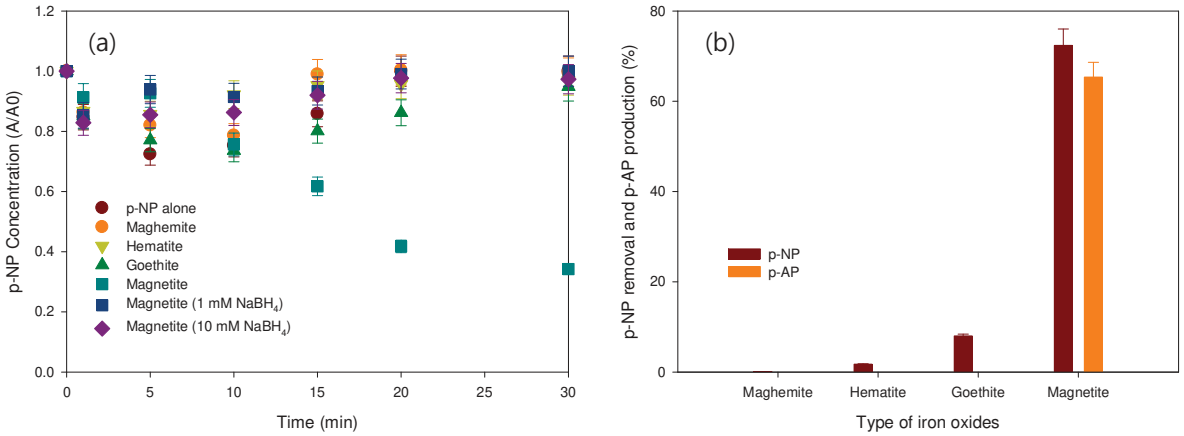

Fig. 8.

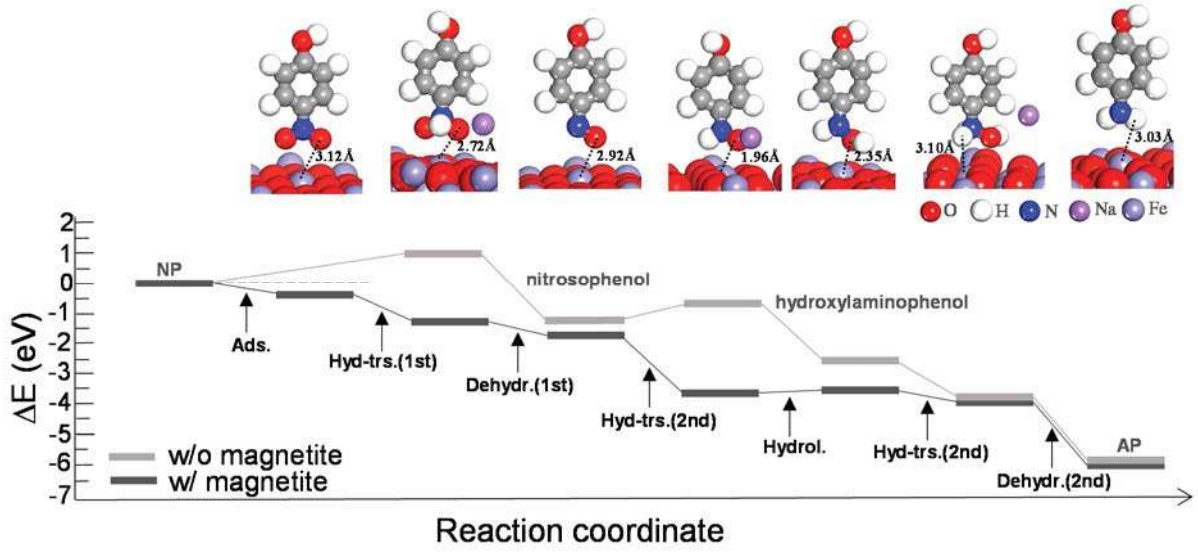

Fig. 9

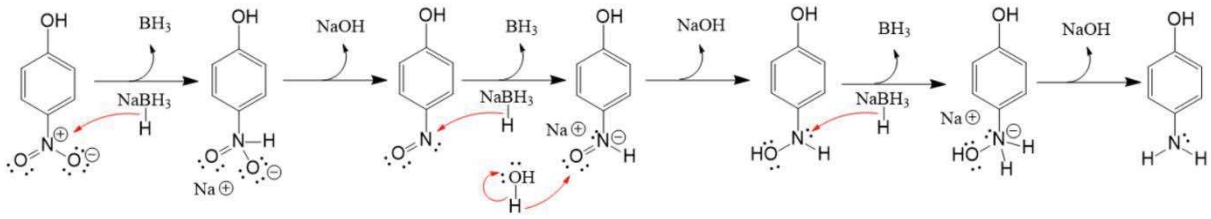

Fig. 10.